ELSEVIER

Contents lists available at ScienceDirect

# Journal of Terramechanics

journal homepage: www.elsevier.com/locate/jterra



# Sensitivity analysis of tire-ice friction coefficient as affected by tire rubber compound properties



Hoda Mousavi\*, Corina Sandu

Terramechanics, Multibody, and Vehicle Systems (TMVS) Laboratory, Department of Mechanical Engineering, Virginia Tech, Blacksburg, VA 24061, United States

#### ARTICLE INFO

Article history: Received 7 February 2020 Revised 5 June 2020 Accepted 19 August 2020

Keywords:
Tire modeling
Sensitivity analysis
Rubber compounds
Terramechanics
Tire test
Water film
Tire-ice model
Viscous friction
Tire friction

# ABSTRACT

Previous studies show that the material properties of the rubber are among the most important factors when designing a tire. In this study, we investigated the effects of different rubber properties on tire performance on ice. A theoretical model that incorporates these tire material properties was developed. The model was used to estimate the height of the water film generated due to friction and the friction coefficient for both, dry and wet regions at the tire-ice contact patch. After validating the results using experimentally collected data, the model was used to perform a sensitivity analysis on the tire performance with respect to six material properties of the tread rubber: thermal conductivity, rubber density, Young's modulus, specific heat, roughness parameter of the rubber, and radii of spherical asperities of the rubber. To study the effect of each parameter, the desired material property was varied within a specific range while the other parameters were kept constant. The results from this study show the sensitivity of the magnitude of the friction coefficient to the rubber material properties. The friction coefficient has a direct relationship with the density of the rubber and has an inverse relationship with Young's modulus, specific heat, and roughness parameter.

© 2020 ISTVS. Published by Elsevier Ltd. All rights reserved.

# 1. Introduction

Tire parameters play a very important role in tire performance. Depending on the driving conditions for which a given tire is designed, its parameters must be chosen appropriately (e.g., the radius of the tire, the width of the tire, material properties of different sections). To understand the effect of tire parameters on its functionality on different types of the terrain, several studies have been conducted (Bhoopalam et al., 2014, Bhoopalam et al., 2015a,b, Bhoopalam et al., 2016, Savitski et al., 2017, Jimenez and Sandu, 2020).

In Mashhadi et al. (2015), the researchers used a finite element approach to perform sensitivity analysis on tire performance with respect to different tire physical parameters, such as radius, width, etc. Another study (Liang et al., 2019) shows the effect of the contact area properties on the tire performance for different slip ratios.

Although there are several studies on tire parameters used to design a tire, only a few of them focus on tire-ice interaction. Mousavi et al. (2019) present the effects of parameters such as tire inflation pressure and the applied normal load on tire performance. In the Mousavi et al. (2019) study, several tests were conducted for

E-mail addresses: hoda13@vt.edu (H. Mousavi), csandu@vt.edu (C. Sandu).

a free-rolling tire. Ivanović et al. (2006) investigated the influence of parameters such as tire forces and vehicle speed on the friction dynamics in the tire contact area using an experimental approach. The results of Makkonen and Tikanmäki (2014) show that there is dry friction in the tire-ice contact area if the vehicle speed or the temperature of the ice is low.

The effect of different tread compounds on tire-ice friction has been investigated by (Roberts, 1981). He mainly focused on the influence of the glass transition temperature when the tire is in contact with ice at different temperatures. The glass transition temperature, which can be measured in terms of the stiffness, is the range of the temperature by which a polymer layer changes from a rigid glassy material to a soft material (Becker and Locascio, 2002).

The amount of water created at the contact patch due to the increase in the temperature is an important parameter that should be taken into account when one wants to study the tire-ice interaction. The frictional force at the contact patch generates heat, so it increases the temperature of the tread and ice. The increase in the temperature of the ice causes the melting of some of the ice, thus creating water. This layer of water on the ice changes the nature of the friction at the contact patch from dry to a combination of viscous and dry friction. Thus, to study the friction coefficient at the tire-ice contact patch, it is essential to determine the parameters that affect the amount of water created at the contact patch.

<sup>\*</sup> Corresponding author.

R

#### Nomenclature

- S Longitudinal slip ratio [-]  $\omega$  Wheel angular velocity [rad/s] V Longitudinal velocity of wheel [m/s]  $\nabla z$  Mean root square gradient [-]
- Ir Standard deviation of the asperity height distribution z height of the spherical asperities [ $\mu$ m]

Giessler et al. (2010) focused on the effect of ambient temperature on tire-ice interaction using an experimental approach. Wiese et al. (2012) developed a theoretical model in order to obtain the viscous friction coefficient at the contact area of a sample rubber block with ice. They found that the obtained friction coefficient varies for different types of rubber.

Radii of the spherical asperities [µm]

The objective of this study is to assess the effect of various rubber material properties on tire performance for tires on ice. In this work, a theoretical tire-ice contact model was developed. The model was used to perform a sensitivity analysis on frictional forces within the tire-ice interaction area with respect to the material properties of the tread section of the tire. Six material properties of the tread part of the tire were considered. To perform the sensitivity analysis, one parameter at a time was changed.

The new model, ATIIM2.0, is the combination and improved version of the previously developed models TIM (Bhoopalam et al., 2016) and ATIIM (Jimenez and Sandu, 2019). The ATIIM2.0 has two main advantages. First, it can predict the friction coefficient at both, dry and wet regions. Second, the model incorporates a larger number of material properties of the tread than there were considered in previous models. Thus, it is better suited to study the influence of different rubber compounds properties on tire performance. The model was validated using the experimental data as presented in (Mousavi and Sandu, 2020a,b). The input data and the data needed for validation were obtained experimentally at the Terramechanics, Multibody, and Vehicle Systems (TMVS) lab at Virginia Tech.

# 2. ATIIM2.0 input data

Several inputs are required for ATIIM2.0 in order to estimate the friction coefficient. We can classify the inputs into three main categories: 1- Data related to material properties of the tread section of the tire, which include: thermal conductivity, density, Young's modulus, specific heat, and the roughness parameters of the rubber surface; 2- The tire-ice pressure distribution at the contact patch; 3- The temperature changes that occur when the tire is in contact with ice. These data have been collected in an experimental study (Mousavi and Sandu, 2020a,b).

1- Data related to material properties of the tread section of the

Three 205/55R16 91Q winter tires with the asymmetrical tread design, manufactured by Sumitomo Research Industries, designated as B, C, and G, were used in this study. The material properties of these tires that were sent by a company to us was presented in (Mousavi and Sandu, 2020a,b). The values of density, Young's modulus, and specific heat of the tread part of the tires that are provided by the company are given in Table 1.

As it is shown in table tire B has the lowest values, and tire C has the next-to-lowest values of specific heat and Young's modulus. For thermal conductivity, a constant value of 0.3 W/m K, which

**Table 1**Material properties of tire B, C, and G.

	Tire B	Tire C	Tire G
Specific heat (kJ/kg K)	1.87	2.13	2.24
Young's Modulus (MPa)	3.3783	4.1909	6.1419
Density (kg/m3)	1103	1094	1137

was given by the company, was used. For the tread roughness parameters, the radii (R) and height (z) of the spherical asperities that are the high spots on the surfaces of the rubber are required. The shapes, deformational characteristics, and forms of these asperities play an important role in the contact mechanics of two bodies in contact with each other (Blau, 2013), Using these two parameters, the mean root square gradient ( $\nabla z$ ) and the standard deviation of the asperity height distribution (lr), which is referred to roughness parameter in this study, can be obtained by Eqs. (1) and (2) (Wiese et al., 2012).

$$lr = \sqrt{\langle z(x)^2 \rangle} \tag{1}$$

$$\nabla z \approx \sqrt{lr/R}$$
 (2)

where z(x) is the height profile of the asperities and  $\langle\rangle$  denotes the average over x.

In this study, the values of the mean root square gradient ( $\nabla z$  = 0.35) and the roughness parameter (lr = 6.5  $\mu$ m) were taken from the literature (Wiese et al., 2012).

# 2- Pressure distribution at the contact patch

The pressure distribution data at the contact area was collected using a TekScan Pressure Pad 3150 (Tekscan, Inc., South Boston, Mass. Pressure Mapping Sensor, 2019). Pressure Pad was attached to a wooden platform the metal U-channels to secure the pad in place. A thin protective film was attached to the top surface of the pressure pad. Thus the surface beneath the TekScan was a smooth rigid surface Fig. 1.

For the calibration of the pressure pad, an equilibrator shown in Fig. 2 was used to apply a uniform known load. The pressure pad was placed into the equilibrator. The equilibrator applies a uniform pressure load using an air compressor.

After calibration, the desired normal load and slip ratio were applied on the tire. Several tests were conducted at TMVS for the desired conditions to collect the required data for all three tires B, C, and G, in free-rolling, traction (with a slip ratio from 2% to 15%), and braking conditions while the tire was on the pressure pad. The protective film placed on the pressure pad helped in protecting the pad for testing under different slip ratios. Fig. 3 shows the pressure distribution for tire B at 4% (a) and 15% (b) slip ratios. Fig. 3 shows the pressure distribution for tire B at 4% (a), and 15% (b) slip ratios.



Fig. 1. Tekscan pressure pad mounting.

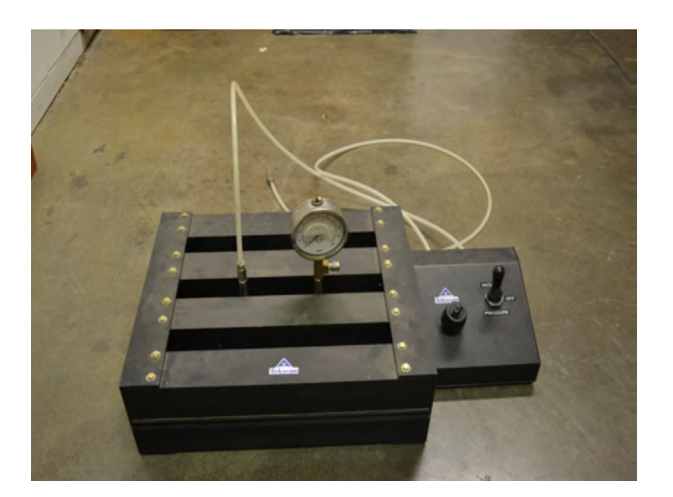


Fig. 2. Tekscan R equilibrator for the pressure pad (Tekscan, Inc., South Boston, Mass)

# 3- Temperature changes at the contact area.

Another parameter that was collected during the test is the temperature in the contact patch of the tire. As shown in Fig. 4, eight thermocouples were installed along the tread of the tire and were connected to data loggers to monitor the temperature of the footprint precisely. Considering the point that tire material

properties are highly dependent on temperature, having the knowledge about how temperature will change at foot print section and tread area will help us to predict the changes in the material properties of the rubber compounds to better predict tire behavior in contact with ice in different ice and environmental temperatures.

The collected temperature changes at the contact patch were used to match and validate the results obtained by ATIIM2.0 for the temperature changes at the contact patch. The ATIIM2.0 has two parameters in its structure that need to be modified using data collected by the experimental approach for the temperature changes to have an accurate estimation of the temperature changes at the contact area.

#### 3. Simulation

ATIIM2.0 is a semi-empirical tire-ice model. This model is an improved version of the combination of the previously developed models (TIM and ATIIM) at TMVS. The initial version of the tire-ice model (TIM) developed by Bhoopalam et al. (2016) can calculate the temperature rise at the contact patch. In this model, using the obtained values of the temperature changes and solving the equation for thermal balance at the tire contact, the friction coefficient at the contact area can be calculated. As TIM did not consider the influence of the water film generated at the tire-ice contact area, the results obtained for the wet traction are not as accurate as those obtained for dry friction.

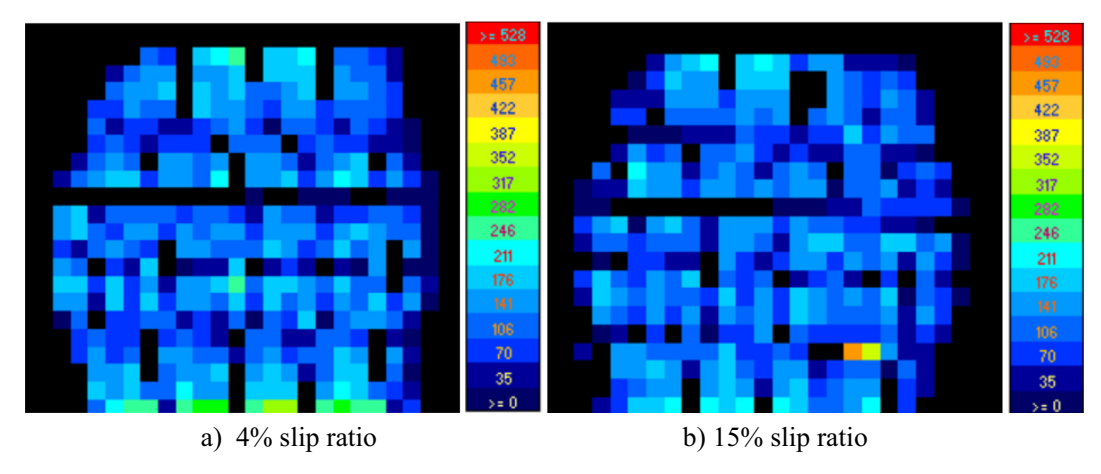


Fig. 3. Pressure distribution for tire B at 4% (a), and 15% (b) slip ratios. The left-right direction here is the longitudinal direction of the tire.



Fig. 4. Eight thermocouples installed to monitor the temperature changes at tread.

To solve this drawback of the TIM, Jimenez and Sandu (2019) developed another model (ATIIM) by adding several moduli to the TIM to take into account the effect of the height of the water film generated at the contact area. Although ATIIM is thus an appropriate model to predict the friction for the wet area, it has two limitations. This model was not able to estimate the equivalent (or total) friction coefficient of the tire for the condition in which we have both dry and wet regions in the contact area. The second limitation is that ATIIM incorporates only three material properties of the tire rubber compounds: thermal conductivity, density, and specific heat of the rubber. Thus, it needed to be expanded to account for multiple rubber compound properties, to be able to benchmark the performance of tires with different rubber compounds.

To eliminate the limitations of TIM and ATIIM, a new model, ATIIM2.0, was developed. In this model, to incorporate more material properties into the model, a new approach to predict the water film created in the contact patch was implemented. The ATIIM2.0 requires six material parameters of the rubber compounds as inputs into the model: tread roughness parameter, tread rubber radii of asperities, rubber compound density, thermal conductivity, Young's modulus, and specific heat. Using the data collected for the height of water film generated at the tire-ice interface, and for the pressure distribution at the contact patch, the viscous friction coefficient at the tire-ice contact area was calculated. In addition, by improving the approach used in TIM to predict the dry friction coefficient, ATIIM2.0 is able to predict the dry friction coefficient in the dry area.

Since quite often, the contact patch area includes both dry and wet regions, a method was needed to obtain the equivalent friction coefficient. In ATIIM2.0, to find the equivalent friction coefficient, the area of each of the wet and dry regions was calculated. Next, using the total area of the contact patch, Eq. (1) is proposed to calculate the total (equivalent) friction coefficient at the contact patch (Mousavi and Sandu, 2020c).

Here are Eqs. (3) and (4):

$$\mu_{Total(avg)} = A_r.\mu_{Viscous(avg)} + (1 - A_r).\mu_{Dry(avg)}$$
(3)

where

$$A_r = \frac{Area \text{ of the wet region } (A_w)}{Total \text{ area of the contact patch } (A_f)} \tag{4}$$

# 4. Results from simulation

This section illustrates the capabilities of ATIIM2.0 by presenting the simulation results obtained for tire C. ATIIM2.0 is able to

calculate: the friction coefficient at wet and dry regions (viscous and dry), the total friction coefficient in the tire-ice contact area, the height of the water film generated in the contact area, the temperature rise in the contact area, the areas of wet and dry regions, and the pressure distribution in the tire-ice contact area. Material properties of tire C were used as inputs into ATIIM2.0 (Mousavi and Sandu, 2020a,b,c). In addition, data collected experimentally using a Tekscan Pressure Pad 3150 for the pressure distribution in the contact area was employed to calculate the temperature changes in the contact area. Fig. 5 presents the results for the average values of viscous and dry friction, and the value of the total friction coefficients within the contact area, obtained using ATIIM2.0 for tire C for different slip ratios (2%, 4%, 8%, 10%, 12%, and 15%) with an inflation pressure of 145 kPa and an applied normal load of 4 kN. The temperature of the ice assumed to be  $-1^{\circ}$ C. Using ATIIM2.0, each type of friction coefficient (viscous and dry) can be estimated at various points in the contact patch (corresponding to the number of the pixels and the dimension of the pressure pad used for collecting the pressure distribution data). The data represented in this plot for the viscous and dry friction were obtained as the average of the values of the respective type of friction coefficient for all the points within the contact area for that specific slip ratio.

The friction coefficient of the wet region (viscous friction) has an increasing trend with the change in the slip ratio from 0% to 15% (Fig. 5). This result confirms results presented by other studies (Bhoopalam et al., 2016), (Kandeva and Dishovsky, 2019). As expected, dry friction coefficients have higher values than viscous friction coefficient and the total friction coefficients which is the equivalent friction coefficient in the contact area and is obtained using Eq. (3). The total friction coefficient has a decreasing trend for lower slip ratios (s < 8%) and will remain almost constant, with small fluctuations, for higher slip ratios.

By increasing the slip ratio, although the magnitude of the viscous friction coefficient increases, there is a general decreasing trend for the total friction coefficient. The reason for this phenomenon is that by increasing the slip ratio, the area of the wet region also increases. By increasing the area of the wet region, the viscous friction contributes more to the value of the total friction, and this causes a decline in the value of the total friction coefficient.

Figs. 6–10 show results for temperature changes, the height of water film, the wet and dry regions, the pressure distribution, and the distribution of the viscous friction coefficient for tire C with 8% slip ratio, as predicted by ATIIM2.0.

A general increasing trend from the leading edge to the trailing edge can be observed for the temperature rise in the contact area.

As expected, by increasing the temperature rise at the tire-ice contact patch, the height of the water film generated is greater at the trailing edge than at the leading edge.

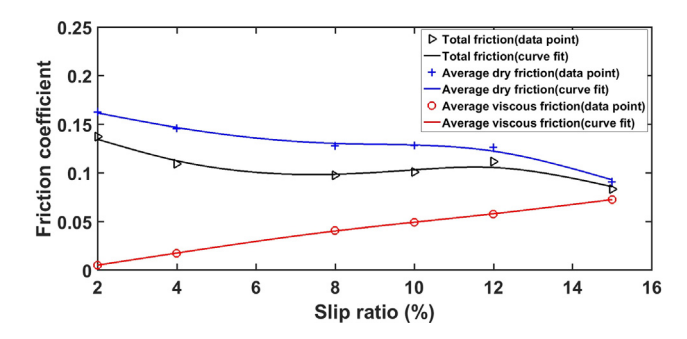


**Fig. 5.** Simulation results for tire C (load = 4 kN and inflation pressure = 145 kPa) for dry, viscous, and total friction coefficient.

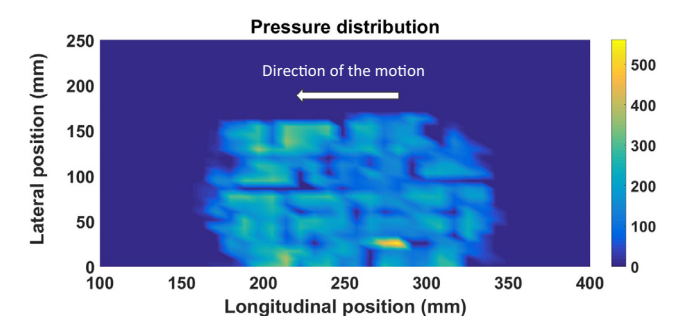


**Fig. 6.** Pressure distribution (Pa) at the contact area modeled by ATIIM2.0 for tire C (load = 4 kN and inflation pressure = 145 kPa) at 8% slip ratio.

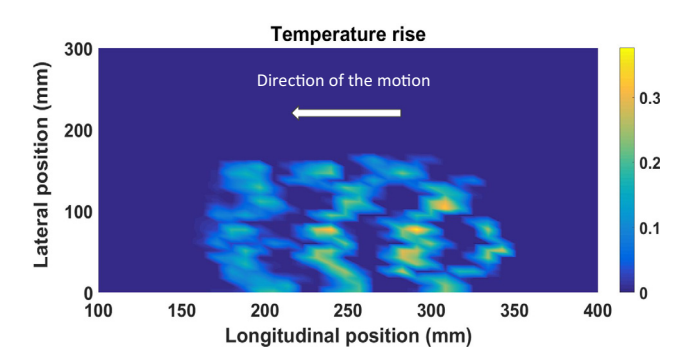
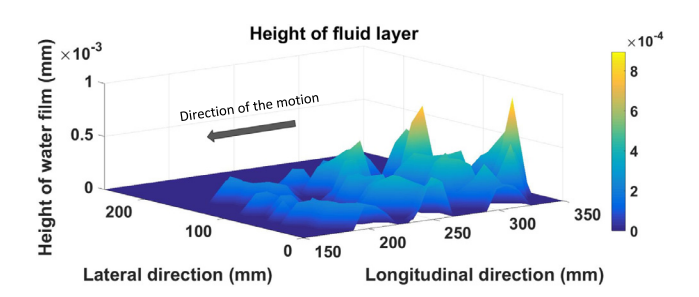
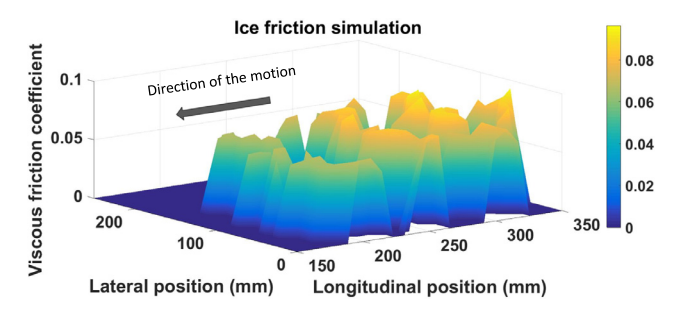


Fig. 7. Temperature rise ( $^{\circ}$ C) at the contact area modeled by ATIIM2.0 for tire C (load = 4 kN and inflation pressure = 145 kPa) at 8% slip ratio.



**Fig. 8.** Height of the water film (h) at the contact area modeled by ATIIM2.0 for tire C (load = 4 kN and inflation pressure = 145 kPa) at 8% slip ratio. Color bar denotes the height of water film, and units are mm.



**Fig. 9.** Distribution of viscous friction coefficient at the contact area modeled by ATIIM2.0 for tire C (load = 4 kN and inflation pressure = 145 kPa) at 8% slip ratio.

As it can be observed from Fig. 9, the viscous friction coefficient is higher at the trailing edge of the contact area.

Fig. 10 shows that most of the water generated at the contact area is close to the trailing edge.

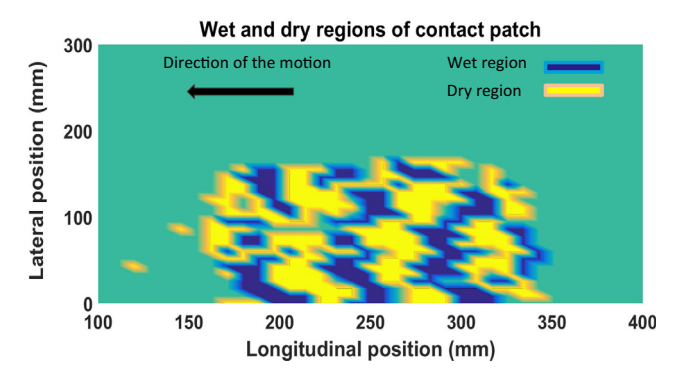


**Fig. 10.** Wet and dry regions at the contact area modeled by ATIIM2.0 for tire C (load = 4 kN and inflation pressure = 145 kPa) at 8% slip ratio.

# 5. Testing setup

The results obtained by the ATIIM2.0 simulation were validated against experimental data collected using the Terramechanics Rig at TMVS (Khan and Sandu, 2017), (Sandu et al., 2008). Several tests were conducted for three tires with different rubber compounds. The other tire parameters, such as the tire radius, width, etc. are identical for all three tires. They are manufactured by the same company. The results for the values of the friction coefficients and the drawbar pull coefficient for all three tires are presented in (Mousavi and Sandu, 2019). The tests were conducted for several testing conditions and different driving modes: free-rolling, traction, and braking conditions. For the traction mode, the slip ratios varied from 2% to 15%. The slip ratio can be created by changing the wheel angular velocity while maintaining constant wheel linear speed. Eq. (5) was used to obtain the angular velocity required to have the desired specific slip ratio of the Terramechanics Rig at TMVS. The linear speed of the rig was kept constant (Meyer et al., 1977; Mousavi and Sandu, 2020b; He et al., 2020).

$$S = \frac{R_e \omega - V}{R_e \omega} \tag{5}$$

where V is the linear speed of the wheel and  $\omega$  is its angular velocity. The effective rolling radius of the tire R<sub>e</sub>was obtained using Eq. (4):

$$R_{e} = \frac{\sin\left(\cos^{-1}\left(\frac{R_{L}}{R_{f}}\right)\right)}{\cos^{-1}\left(\frac{R_{L}}{R_{f}}\right)} * R_{f} \tag{6}$$

where Rf and RL are the unloaded radius and loaded radius of the tire, respectively. The radii Rf and RL were measured for all three tires according to the design of the experiment for three sets of operational conditions. The tire nominal inflation pressure for the candidate tires with the nominal normal load of 7kN is 241 kPa. For this study, 80% and 60% of the nominal loading and nominal inflation pressure were chosen as the operational condition of the tests. The three sets of operating conditions were 5.6 kN normal load and 193 kPa tire inflation pressure (80% of the nominal values) when the tire temperature was at  $-1^{\circ}$ C, 5.6 kN normal load and 193 kPa tire inflation pressure when the tire temperature was at  $-5^{\circ}$ C, and 4 kN normal load and 145 kPa tire inflation pressure (60% of the nominal values) when the tire temperature was at  $-1^{\circ}$ C. The measured values for Rf and RL were used in estimating effective rolling radius (Re) using Eq. (4), which is derived from lazar (2017).

To validate ATIIM2.0 for temperature changes at the contact area, eight thermocouples were mounted on the tread of each tire to measure the temperature changes during the contact of the tire with the ice. For each test, the ice surface was prepared to have the

same value of the static friction coefficient  $\sim$  0.1, which was used later as an input for the ATIIM2.0. Before conducting the test, the tire was cooled down to the temperature below the ice temperature ( $-20~^\circ\text{C}$ ) using a cooler. During the mounting process of the tire on the testing rig, the tire temperature increases (due to the heat transfer with higher ambient temperature). To test a tire with the desired temperature ( $-10~^\circ\text{C}$  and  $-5~^\circ\text{C}$  for this study), the temperature of the mounted tire monitored frequently. When the temperature of the tire reached to the desired temperature, the test was conducted. The temperature of the tire was monitored using thermocouples mounted on the tread part of the tire. The ice temperature was controlled and was set to a constant value using thermocouples and chiller for the desired temperature. Figs. 11–13 show results obtained for all three tires.

These results were obtained under three conditions:

- 1. The temperature of the ice and of the tire was -10 °C, the tire inflation pressure was 193 kPa base on the design of the experiment, and the normal load applied on the wheel was 5.6 kN.
- 2. The temperature of the ice was -10 °C, the temperature of the tire was -5°C, the tire inflation pressure was 193 kPa, and the normal load applied on the wheel was 5.6 kN.
- 3. The temperature of the ice and of the tire was  $-1^{\circ}$ C, the tire inflation pressure was 145 kPa, and the normal load applied on the wheel was 4 kN.

For all three tires, the value of the longitudinal force decreases when the tire temperature increases (Figs. 11–13). For each of the three conditions and for the range of slip ratios from 0 to 30%, the drawbar pull coefficient was greatest for tire B, was intermediate for tire G, and was least for tire C.

#### 6. Sensitivity analysis

For the sensitivity analysis of the performance criteria modeled by ATIIM2.0 with respect to the different tread rubber parameters, one model parameter was changed at a time, while keeping the other parameters constant. In this study, the sensitivity of the model, with respect to six parameters of the tread rubber was investigated: thermal conductivity, Young's modulus, specific heat, density, and roughness. Figs. 14 and 15 show the average viscous and dry friction coefficients for tire B obtained with ATIIM2.0 for different rubber thermal conductivity values (k). As shown in Fig. 14, by increasing the rubber thermal conductivity, the value of the average viscous friction coefficient increases slightly. An increase was observed in the values of the average dry friction

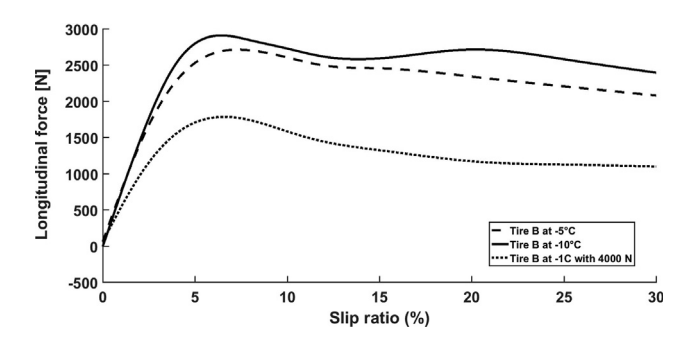


**Fig. 11.** Longitudinal force for tire B for three testing conditions: 1: The temperatures of the ice and tire were  $-10\,^\circ\text{C}$ , the inflation pressure was 193 kPa and 5.6 kN normal load was applied on the wheel. 2: The temperature of the ice was  $-10\,^\circ\text{C}$  and the temperature of the tire was  $-5\,^\circ\text{C}$ , the inflation pressure was 193 kPa and 5.6 kN normal load was applied on the wheel. 3: The temperatures of the ice and tire were  $-1\,^\circ\text{C}$ , the inflation pressure was 145 kPa and 4 kN normal load was applied on the wheel.

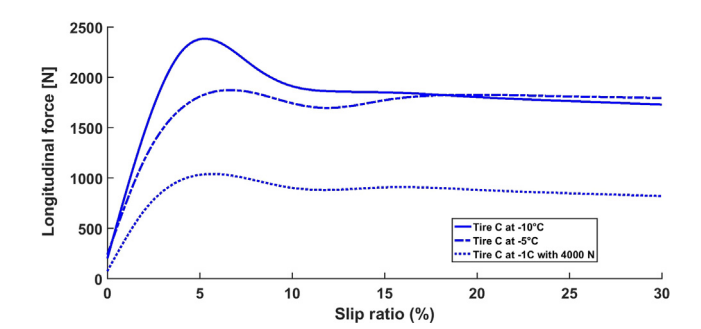


**Fig. 12.** Longitudinal force for tire C for three testing conditions: 1: The temperatures of the ice and tire were  $-10\,^{\circ}$ C, the inflation pressure was 193 kPa and 5.6 kN normal load was applied on the wheel. 2: The temperature of the ice was  $-10\,^{\circ}$ C and the temperature of the tire was  $-5\,^{\circ}$ C, the inflation pressure was 193 kPa and 5.6 kN normal load was applied on the wheel. 3: The temperatures of the ice and tire were  $-1\,^{\circ}$ C, the inflation pressure was 145 kPa and 4 kN normal load was applied on the wheel.

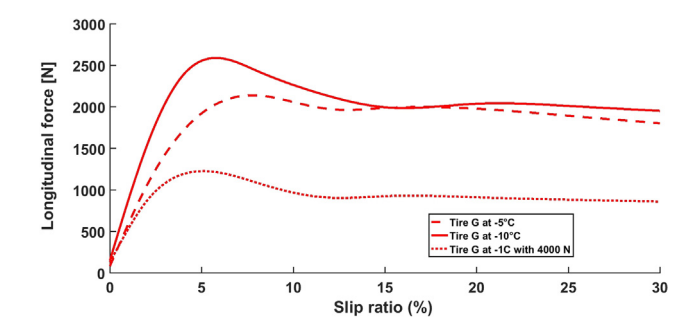


**Fig. 13.** Longitudinal force for tire G for three testing conditions: 1. The temperatures of the ice and tire were  $-10\,^\circ\text{C}$ , the inflation pressure was 193 kPa and 5.6 kN normal load was applied on the wheel. 2. The temperature of the ice was  $-10\,^\circ\text{C}$  and the temperature of the tire was  $-5\,^\circ\text{C}$ , the inflation pressure was 193 kPa and 5.6 kN normal load was applied on the wheel. 3. The temperatures of the ice and tire were  $-1\,^\circ\text{C}$ , the inflation pressure was 145 kPa and 4 kN normal load was applied on the wheel.

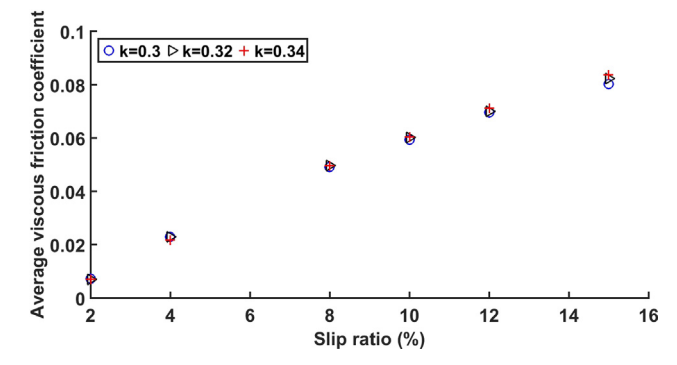


**Fig. 14.** ATIIM 2.0 simulation results for mean value of viscous friction coefficient for tire B for different rubber thermal conductivity values (k (W/m·K)). Nominal load of 4 kN, inflation pressure of 144.79 kPa, static friction coefficient  $\sim$ 0.1, and ice temperature of -1 °C.

coefficient when the thermal conductivity was increased for some of the slip ratios (2%, 4%, and 10%). While at 8% and 12%, a decreasing trend can be observed. As it is shown in Fig. 15 and Fig. 16, by increasing the thermal conductivity, the dry and total friction coefficient decreased slightly or remained unchanged.

Fig. 17 shows the average viscous friction coefficient for tire B obtained using ATIIM2.0 for different rubber Young's modulus values. As shown in Fig. 17, Figs. 18, and 19, by increasing the rubber modulus of elasticity, the value of the average friction coefficients

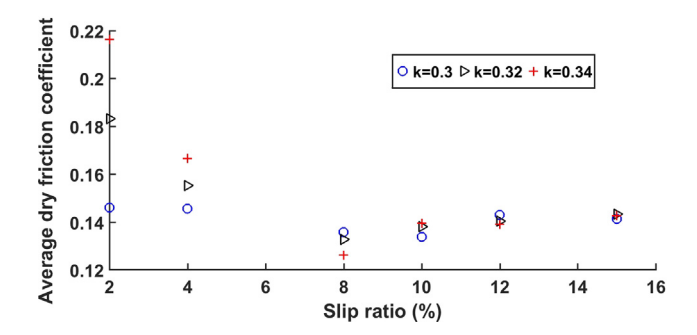


**Fig. 15.** ATIIM 2.0 simulation results for mean value of dry friction coefficient for tire B for different rubber thermal conductivity values (k (W/m·K)). Loaded Nominal load of 4 kN, the inflation pressure of 145 kPa, the static friction coefficient  $\sim$ 0.1, and the ice temperature of -1 °C.

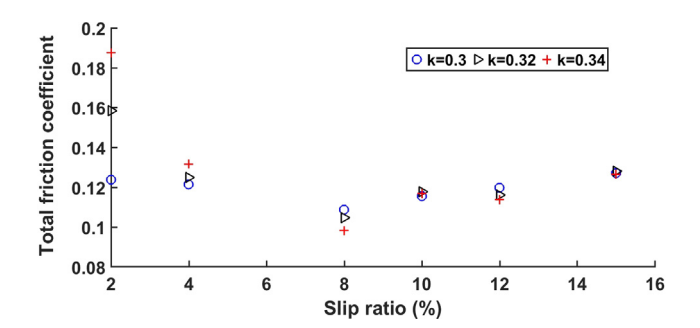


**Fig. 16.** ATIIM 2.0 simulation results for value of total friction coefficient for tire B for different rubber thermal conductivity values (k (W/m·K)). Loaded Nominal load of 4 kN, the inflation pressure of 145 kPa, the static friction coefficient  $\sim$ 0.1, and the ice temperature of -1 °C.

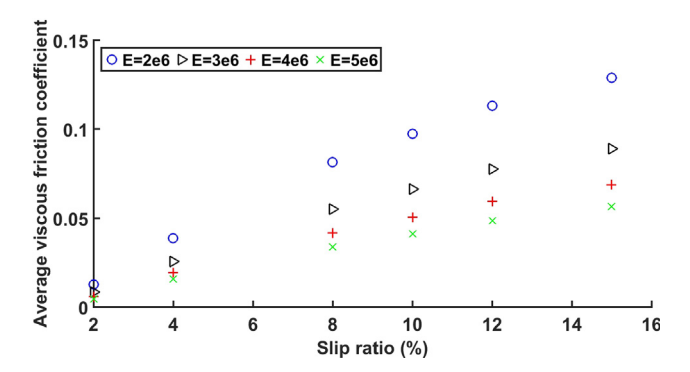


**Fig. 17.** ATIIM 2.0 simulation results for mean value of viscous friction coefficient for tire B for different rubber Young's modulus values (E (Pa)). Nominal load of 4 kN, inflation pressure of 145 kPa, the static friction coefficient  $\sim$ 0.1, and the ice temperature of -1 °C.

for viscous and dry, and the value of the total friction coefficient decreased. Furthermore, the difference in the value of the viscous friction coefficient shows that for the smaller value of Young's modulus, we have a greater distance between the values of the viscous friction coefficient. According to the experimental results, tire B with the smallest Young's modulus has the highest friction coefficient in both, simulation and experiment. In addition, the graph shows that the small change in the Young's modulus parameter results in a large change in the friction coefficient. In other word, the Young's modulus has an important effect on the tire performance (see Figs. 18 and 19).

Fig. 20 shows the average viscous friction coefficient for tire B obtained using ATIIM2.0 for different rubber specific heat values (C). As shown in Fig. 20, by increasing the specific heat of the rub-

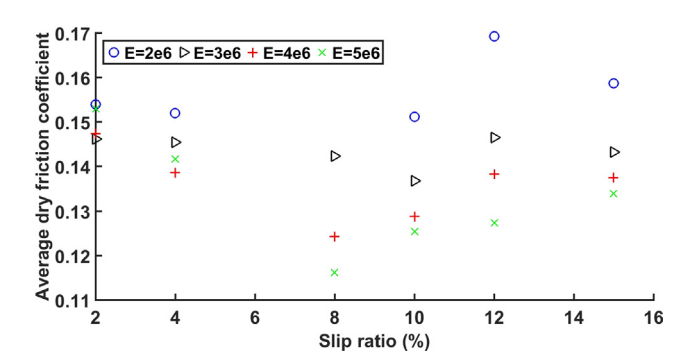


**Fig. 18.** ATIIM 2.0 simulation results for mean value of dry friction coefficient for tire B for different rubber Young's modulus values (E (Pa)). Loaded Nominal load of 4 kN, the inflation pressure of 145 kPa, the static friction coefficient  $\sim$ 0.1, and the ice temperature of -1 °C.

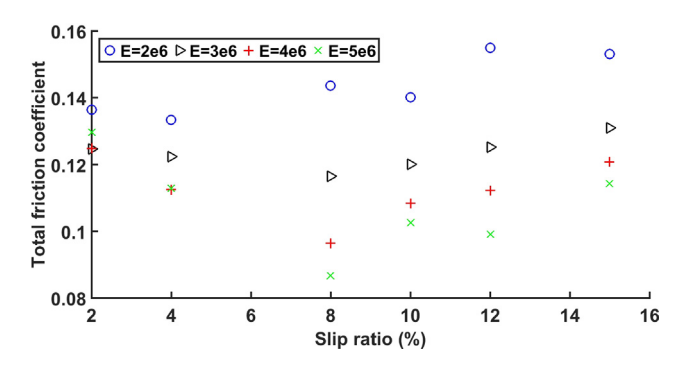


**Fig. 19.** ATIIM 2.0 simulation results for value of total friction coefficient for tire B for different rubber Young's modulus values (E (Pa)). Loaded Nominal load of 4 kN, the inflation pressure of 145 kPa, the static friction coefficient  $\sim$ 0.1, and the ice temperature of -1 °C.

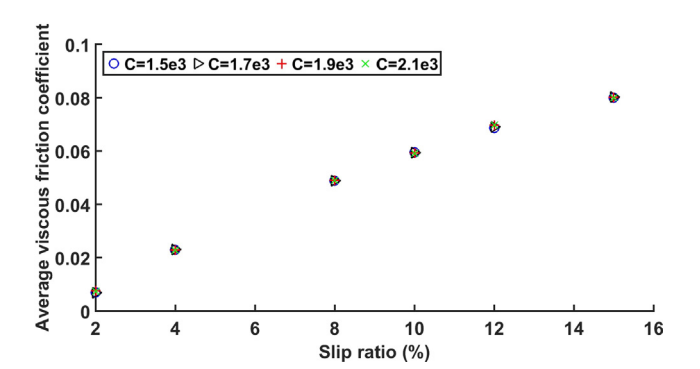


**Fig. 20.** ATIIM 2.0 simulation results for mean value of viscous friction coefficient for tire B for different rubber specific heat values (C (J/kg°C)). Loaded Nominal load of 4 kN, the inflation pressure of 145 kPa, the static friction coefficient  $\sim$ 0.1, and the ice temperature of -1 °C.

ber, the value of the average viscous friction coefficient decreases slightly. As shown in Figs. 21 and 22, for the majority of the slip ratios (2%, 4%, 10%, and 15%), a decreasing trend was observed for the average value of the dry friction coefficient and the total friction coefficient of the tire when the specific heat values increases. Tire B had the smallest specific heat parameter among the three tires tested and also had the highest friction coefficient value. This result was expected. However, as shown in Fig. 17, the effect of Young's modulus can negate the effect of specific heat on the friction coefficient at higher slip ratios. Thus, the equivalent friction coefficient is following the trend for different Young's mod-

ulus for higher slip ratios and is higher for tire B than it is for the other two tires. The difference between the values of the total friction coefficient for two consecutive values of the C is smaller for higher slip ratios (see Figs. 21 and 22).

Fig. 23 shows the average viscous friction coefficient for tire B obtained using ATIIM2.0 for different rubber density values ( $\rho$ ). By increasing the rubber density, the value of the average viscous friction coefficient decreases. The difference between the values of the viscous friction coefficient for various values of rubber density is relatively small for lower slip ratios. However, the results for dry friction and total friction show a general increasing trend in the values of the friction coefficient when increasing the density for higher slip ratios (see Figs. 24 and 25).

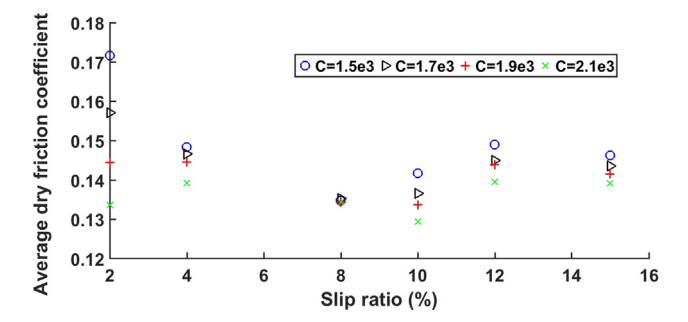
Fig. 26 shows the average viscous friction coefficient for tire B obtained using ATIIM2.0 for different values of the rubber root mean square gradient ( $\nabla z$ ), which is a measure of the roughness parameter of the tread rubber. As shown, in general, by increasing the root mean square gradient, which means a decrease in the radii of the spherical asperities, the average values of the viscous and dry, and the value of the total friction coefficient decrease. For this study, the value of 0.35 found in the literature was used; however, for more precise results, the exact roughness value of each tire should be used (see Figs. 27 and 28).

Fig. 29 shows the average viscous friction coefficient for tire B obtained using ATIIM2.0 for different values of the rubber roughness parameter (lr). By increasing lr, the value of the average viscous friction coefficient increases slightly. For this study, the value of 6.5  $\mu$ m found in the literature was used for lr. As shown, this parameter does not play an important role in the magnitude of the total friction coefficient (see Fig. 30).

#### 7. Conclusion

The main aim of this study was to gain a more thorough understanding of the tire-ice interaction using experimental tests as well as modeling techniques. This article focuses primarily on the investigation of the effect of the rubber compound of pneumatic tire treads on the tire's performance on the ice. Several tests were conducted for three tires labeled as B, C, and G, with different rubber compounds in free-rolling, braking, and traction conditions. The chosen tires are identical in all parameters such as dimensions and tread pattern, except for the tread rubber compounds properties (specific heat, density, Young's modulus, roughness parameters, and thermal conductivity of the tread). A theoretical model was developed to predict the friction coefficient and the height of the water film at the contact area of the tire and ice.

Several tests were conducted for three tires with identical construction and tread pattern, but with different material properties of the tread rubber compounds.



**Fig. 21.** ATIIM 2.0 simulation results for mean value of dry friction coefficient for tire B for different rubber specific heat values (C (J/kg°C)). Loaded Nominal load of 4 kN, the inflation pressure of 145 kPa, the static friction coefficient  $\sim$ 0.1, and the ice temperature of -1 °C.

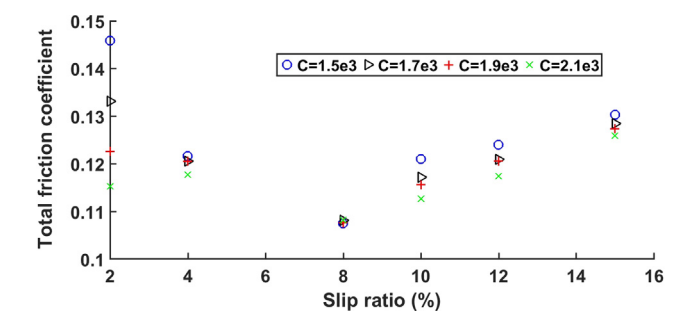


**Fig. 22.** ATIIM 2.0 simulation results for value of total friction coefficient for tire B for different rubber specific heat values (C (J/kg°C)). Loaded Nominal load of 4 kN, the inflation pressure of 145 kPa, the static friction coefficient  $\sim$ 0.1, and the ice temperature of -1 °C.

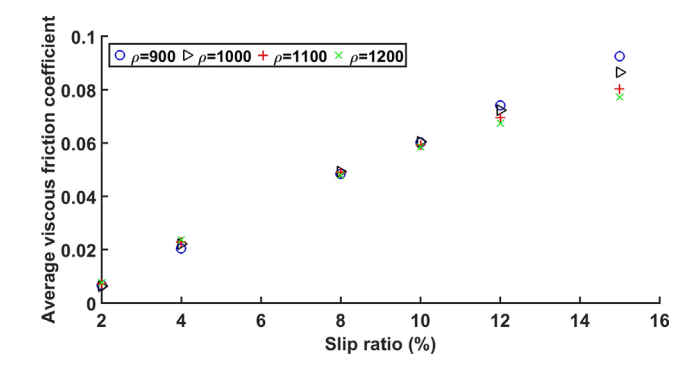


**Fig. 23.** ATIIM 2.0 simulation results for mean value of viscous friction coefficient for tire B for different rubber density values ( $\rho$  (kg/m3)). Loaded Nominal load of 4 kN, the inflation pressure of 145 kPa, the static friction coefficient ~0.1, and the ice temperature of -1 °C.

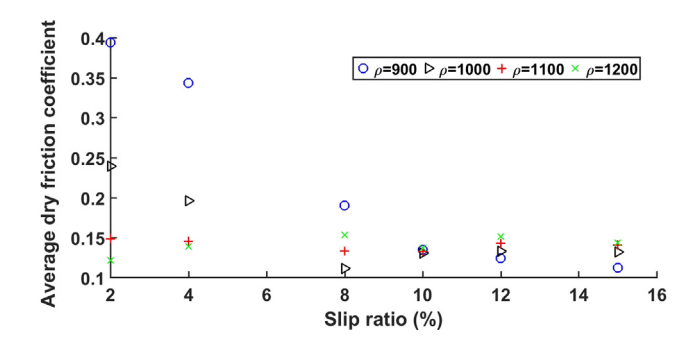


**Fig. 24.** ATIIM 2.0 simulation results for mean value of dry friction coefficient for tire B for different rubber density values ( $\rho$  (kg/m3)). Loaded Nominal load of 4 kN, the inflation pressure of 145 kPa, the static friction coefficient ~0.1, and the ice temperature of -1 °C.

The model ATIIM2.0 is suitable for obtaining dry and viscous friction for both wet and dry regions. In this study, ATTIM2.0 was used to perform a sensitivity analysis to investigate the sensitivity of tire performance with respect to various rubber compound parameters.

From the ATIIM2.0 simulation results, we note that:

- The average values of viscous friction coefficient for tires B, C, and G obtained using ATIIM2.0 is logical considering the static friction coefficient (~0.1) that was measured in the experimental study.
- Among all three tires, tire B shows the highest value of friction coefficients for all cases of viscous, dry, and total friction. Tire C has the next highest value.

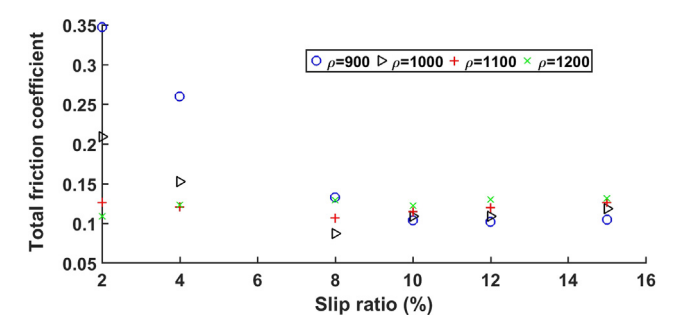


**Fig. 25.** ATIIM 2.0 simulation results for value of total friction coefficient for tire B for different rubber density values ( $\rho$  (kg/m3)). Loaded Nominal load of 4 kN, the inflation pressure of 145 kPa, the static friction coefficient ~0.1, and the ice temperature of -1 °C.

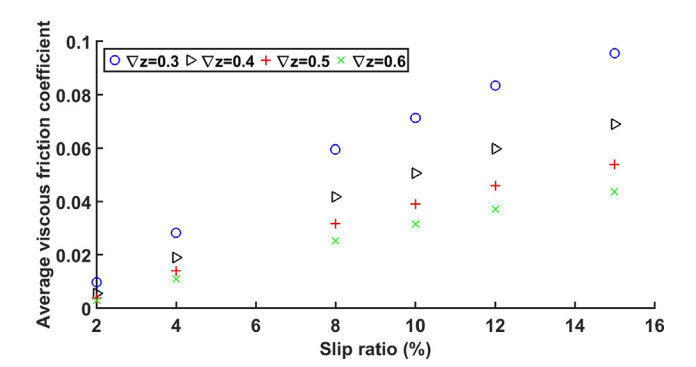


**Fig. 26.** ATIIM 2.0 simulation results for mean value of viscous friction coefficient for tire B for different values of the rubber root mean square gradient ( $\nabla z$ ). Loaded Nominal load of 4 kN, the inflation pressure of 145 kPa, the static friction coefficient ~0.1, and the ice temperature of -1 °C.

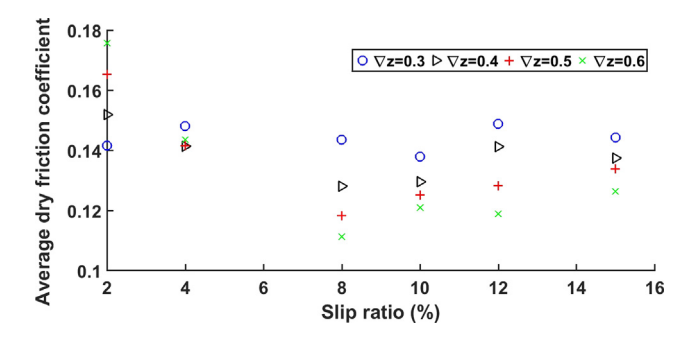


**Fig. 27.** ATIIM 2.0 simulation results for mean value of dry friction coefficient for tire B for different values of the rubber root mean square gradient ( $\nabla$ z). Loaded Nominal load of 4 kN, the inflation pressure of 145 kPa, the static friction coefficient ~0.1, and the ice temperature of -1 °C.

For the sensitivity analysis of the ATIIM2.0 for different rubber parameters, one model parameter was changed at a time while keeping the other parameters constant. Below are the results for the sensitivity analysis obtained for different slip ratios:

- For the majority of the slip ratios used for this study, by increasing the thermal conductivity of the rubber, the value of the total friction coefficient decreased slightly or remained unchanged.
- By increasing the Young's modulus (E) of the rubber, the values
  of friction coefficient (viscous, dry, and total) decreases. Furthermore, the difference in the value of the viscous friction coefficient for two different values of E is larger for smaller values of

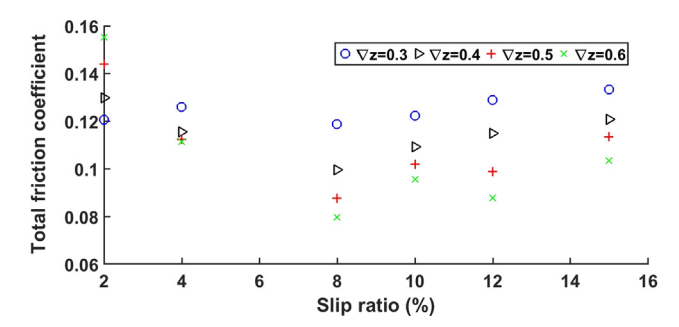


**Fig. 28.** ATIIM 2.0 simulation results for value of total friction coefficient for tire B for different values of the rubber root mean square gradient ( $\nabla z$ ). Loaded Nominal load of 4 kN, the inflation pressure of 145 kPa, the static friction coefficient ~0.1, and the ice temperature of -1 °C.

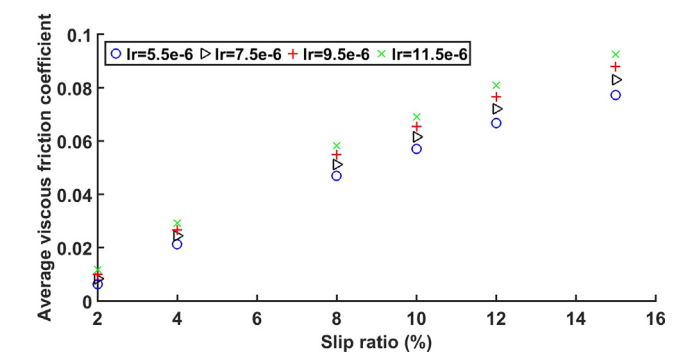


**Fig. 29.** ATIIM 2.0 simulation results for mean value of viscous friction coefficient for tires B for different values of roughness parameter of rubber (lr (m)). Loaded Nominal load of 4 kN, the inflation pressure of 145 kPa, the static friction coefficient  $\sim$ 0.1, and the ice temperature of -1 °C.

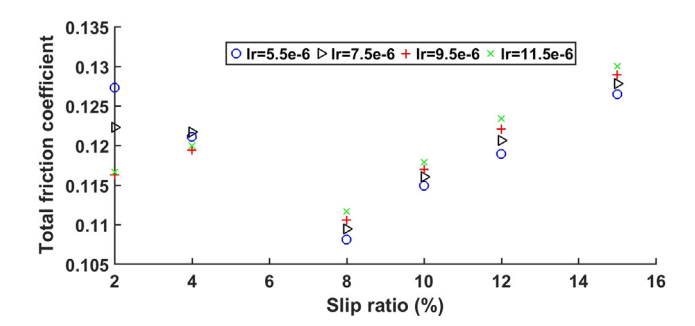


**Fig. 30.** ATIIM 2.0 simulation results for value of total friction coefficient for tire B for different values of the rubber roughness parameter (lr (m)). Loaded Nominal load of 4 kN, the inflation pressure of 145 kPa, the static friction coefficient  $\sim$ 0.1, and the ice temperature of -1 °C.

- E than it is for the larger values of E. Tire B with the smallest value of Young's modulus was shown to have the highest friction coefficient in both, simulation and experiment.
- For the majority of the slip ratios, a decreasing trend was observed for the average value of the dry friction coefficient and the total friction coefficient of the tire when the specific heat values increases.
- By increasing the rubber density, the value of the average viscous friction coefficient decreases. However, the results for dry friction and total friction show a general increasing trend in the values of the friction coefficient when increasing the density of the rubber for higher slip ratios.

- By increasing the roughness parameter of the rubber (the root mean square gradient), the value of the friction coefficient (viscous, dry, and total) decreases.
- By increasing the other roughness parameter of the rubber (lr), the value of the friction coefficient does not change too much.

#### **Declaration of Competing Interest**

The authors declare the following financial interests/personal relationships which may be considered as potential competing interests: The NSF I/UCRC Center for Tire Research (CenTiRe) partially funded this work.

#### Acknowledgments

The authors would like to thank the Terramechanics, Multibody, and Vehicle Systems Laboratory at Virginia Tech for the testing facilities used in this study and the support of the NSF I/UCRC Center for Tire Research (CenTiRe) who partially funded this work. The authors also would like to thank Mr. Mehran Shams for his help during this study and Mr. Mohit Nitin Shenvi for his help in conducting the tests for the experimental study.

#### References

- Becker, H., Locascio, L.E., 2002. Polymer microfluidic devices. Talanta 56, 267–287. https://doi.org/10.1016/S0039-9140(01)00594-X.
- Bhoopalam, A.K., Sandu, C., Taheri, S., 2016. A tire-ice model (TIM) for traction estimation. J. Terramechanics 66, 1–12. https://doi.org/10.1016/j.jterra.2016.02.003.
- Bhoopalam, A.K., Sandu, C., Taheri, S., 2015a. Experimental investigation of the performance of pneumatic tires on ice. Part I Indoor study. J. Terramechanics 60, 43–54. https://doi.org/10.1016/j.jterra.2015.02.006 (12).
- Bhoopalam, A.K., Sandu, C., Taheri, S., 2015b. Experimental investigation of the performance of pneumatic tires on ice. part II Outdoor Study". J. Terramechanics 60, 55–62. https://doi.org/10.1016/j.jterra.2015.03.001 (8).
- Bhoopalam, A.K., Sandu, C., Taheri, S., 2014. Tire traction of commercial vehicles driving on icy roads. SAE Int. J. Commercial Vehicles 7 (2), 357–365. https://doi.org/10.4271/2014-01-2292. 9.
- Blau, P.J., 2013. Asperities. In: Wang, Q.J., Chung, YW. (Eds.) Encyclopedia of Tribology. Springer, Boston, MA. https://doi.org/10.1007/978-0-387-92897-5
- Gießler, Martin, Frank Gauterin, Wiese, K., Wies, B., 2010. Influence of friction heat on tire traction on ice and snow. Tire Science and Technology 38, no. 1, 4–23.
- Meyer, M.P., Ehrlich, I.R., Sloss, D., Murphy, N.R., et al., 1977. International society for terrain-vehicle systems standards. J. Terramech. 14 (3), 153–182.

- Ivanovic, V., Deur, J., Kostelac, M., Herold, Z., et al., 2006. Experimental identification of dynamic tire friction potential on ice surfaces. Veh. Syst. Dyn. 44, 93–103. https://doi.org/10.1080/00423110600869230.
- Jazar, R.N., 2017. Vehicle Dynamics: Theory and Application. Springer.
- Jimenez, E., Sandu, C., 2019. Towards a real-time pneumatic tire performance prediction using an advanced tire-ice interface model. J. Terramechanics 81, 43– 56. https://doi.org/10.1016/j.jterra.2018.04.004.
- Jimenez, E., Sandu, C., 2020. Experimental investigation of the tractive performance of pneumatic tires on ice. Tire Sci. Technol. 48 (1), 22–45. https://doi.org/ 10.2346/tire.18.460409.
- Kandeva, M., Dishovsky, N., 2019. Friction behavior produced in the course of a contact enabled between composite materials and eco-friendly soles prototypes made of elastomeric material with regard to ice-covered surface. Tribol. Ind. 41, 90–99. https://doi.org/10.24874/ti.2019.41.01.10.
- Khan, A.K., Sandu, C., 2017. Design and manufacturing of a clutch and brake system for indoor tire testing. ASME 2017 International Design Engineering Technical Conferences and Computers and Information in Engineering Conference. American Society of Mechanical Engineers Digital Collection.
- He, R., Sandu, C., Mousavi, H., Shenvi, M. N., et al., 2020. Updated standards of the international society for terrain-vehicle systems. J. Terramech. 91, 185–231. https://doi.org/10.1016/j.jterra.2020.06.007.
- Liang, C., Ji, L., Mousavi, H., Sandu, C., 2019. Evaluation of tire traction performance on dry surface based on tire-road contact stress. In SIAR International Congress of Automotive and Transport Engineering: Science and Management of Automotive and Transportation Engineering, 138–152.
- Makkonen, L., Tikanmäki, M., 2014. Modeling the friction of ice. Cold Reg. Sci. Technol. 102, 84–93. https://doi.org/10.1016/j.coldregions.2014.03.002.
- Mashhadi, B., Mousavi, H., Montazeri, M., 2015. Obtaining relations between the Magic Formula coefficients and tire physical properties. Int. J. Automot. Eng. 5, 911–922.
- Mousavi, H., Shenvi, M.N., Sandu, C., 2019. Experimental study for free rolling of tire on ice. ASME 2019 Int. Des. Eng. Tech. Conf. Comput. Inf. Eng. Conf. IDETC/CIE 2019 1–11.
- Mousavi, H., Sandu, C., 2020a. Study on the effects of rubber compounds on tire performance on ice. SAE Tech. Pap., 2020-01-1228, e-ISSN, 2688-3627. https://doi.org/10.4271/2020-01-1228.
- Pressure Mapping Sensor 3150, https://www.tekscan.com/products-solutions/pressure-mapping-sensors/3150, (accessed March 2019)
- Mousavi, H., Sandu, C., 2020b. Tire-ice model development for the simulation of rubber compounds effect on tire performance. Journal of Terramechanics 91, 97–115. https://doi.org/10.1016/j.jterra.2020.06.001.
- Mousavi, H., Sandu, C., 2020c. Experimental Study of Tread Rubber Compound Effects on Tire Performance on Ice. SAE Int. J. Commer. Veh. 13 (2). https://doi.org/10.4271/02-13-02-0006.
- Roberts, A.D., 1981. Rubber-ice adhesion and friction. J. Adhesion 13 (1), 77–86.
- Sandu, C., Taylor, B., Biggans, J., Ahmadian, M., 2008. Building an infrastructure for indoor terramechanics studies: the development of a terramechanics rig at virginia tech. In: Proceedings of 16th ISTVS international conference, Turin, Italy, pp. 177–185.
- Savitski, D., Schleinin, D., Ivanov, V., Augsburg, K., et al., 2017. Improvement of traction performance and off-road mobility for the vehicle with four individual electric motors: Driving over icy road". J. Terramechanics 69, 33–43. https://doi.org/10.1016/j.jterra.2016.10.005 (11).
- Wiese, K., Kessel, T.M., Mundl, R., Wies, B., 2012. An analytical thermodynamic approach to friction of rubber on ice. Tire Sci. Technol. 40, 124–150.